Comparative Anatomy of the Mammalian Neuromuscular Junction

Comparative Anatomy of the Mammalian Neuromuscular Junction

Ines Boehm[1,2]^, Abrar Alhindi[1,2]^, Ana S. Leite[1,2,3], Chandra Logie[4], Alyssa Gibbs[1,2], Olivia Murray[1,2], Rizwan Farrukh[1,2], Robert Pirie[4], Christopher Proudfoot[4], Richard Clutton[4], Thomas M. Wishart[4], Ross A. Jones[1,2]* & Thomas H. Gillingwater[1,2]*

[1]Edinburgh Medical School: Biomedical Sciences, University of Edinburgh, Edinburgh EH8 9AG, UK

[2]Euan MacDonald Centre for Motor Neurone Disease Research, University of Edinburgh, Edinburgh EH8 9AG, UK

[3]School of Medicine, UNESP-São Paulo State University, Campus Botucatu, Botucatu, Sao Paulo, Brazil

[4]The Roslin Institute and R(D)SVS, Easter Bush Campus, University of Edinburgh, Edinburgh, EH25 9RG, UK

^&* These authors contributed equally

Corresponding author:

Professor Thomas H. Gillingwater, University of Edinburgh, Old Medical School (Anatomy), Teviot Place, Edinburgh, EH8 9AG

Email: t.gillingwater@ed.ac.uk

Tel: +44 (0)131 650 3724

Conflict of interest statement: The authors declare no conflicts of interest

Abstract

The neuromuscular junction (NMJ) – a synapse formed between lower motor neuron and skeletal muscle fibre – represents a major focus of both basic and clinical neuroscience research. Although the NMJ is known to play an important role in many neurodegenerative conditions affecting humans, the vast majority of anatomical and physiological data concerning the NMJ come from lower mammalian (e.g. rodent) animal models. However, recent findings have demonstrated major differences between the cellular and molecular anatomy of human and rodent NMJs. Therefore, we undertook a comparative morphometric analysis of the NMJ across several larger mammalian species in order to generate baseline inter-species anatomical reference data for the NMJ, and to identify animal models that better represent the morphology of the human NMJ *in vivo*. Using a standardized morphometric platform ('NMJ-morph') we analysed 5,385 individual NMJs from lower/pelvic limb muscles (EDL, soleus and peronei) of 6 mammalian species (mouse, cat, dog, sheep, pig and human). There was marked heterogeneity of NMJ morphology both within and between species, with no overall relationship found between NMJ morphology and muscle fibre diameter or body size. Mice had the largest NMJs on the smallest muscle fibres; cats had the smallest NMJs on the largest muscle fibres. Of all the species examined, the sheep NMJ had the most closely-matched morphology to that found in humans. Taken together, we present a series of comprehensive baseline morphometric data for the mammalian NMJ and suggest that ovine models are likely to best represent the human NMJ in health and disease.

Keywords: neuromuscular junction; comparative anatomy; NMJ-morph; mammalian; synapse

Introduction

The neuromuscular junction (NMJ) has been a focus of physiological research since the 1800's, representing an ideal, experimentally-accessible, model synapse (Clarac and Pearlstein 2007; Slater 2008, 2015, 2017; Szule et al. 2015; Rudolf et al. 2019). More recently, it has become clear that the NMJ's critical role in signal transmission between lower motor neuron and skeletal muscle fibre makes it a major target in many neurodegenerative and neuromuscular conditions (Murray et al. 2010; Rudolf et al. 2016; Verschuuren et al. 2016; Rodríguez Cruz et al. 2018). Whilst the physiology of the NMJ has been well-studied across a wide range of invertebrate (Clarac and Pearlstein 2007) and vertebrate species, including humans (Wood and Slater 2001), far less is known about comparative NMJ morphology between mammalian species, especially with respect to humans (Jones et al. 2017). Moreover, small mammal animal models remain the mainstay of research into the contribution of the NMJ to many neurodegenerative conditions.

In order to better understand the form and function of the NMJ in health and disease, particularly with regards to humans, it will be important to identify animal models that more closely mimic the human condition. Given the clear differences that have been recently reported in the cellular and molecular composition of human and mouse NMJs (Jones et al. 2017), larger animal models might offer more appropriate alternatives. With major technological advances in gene editing technologies that have arisen over the past decade, there is a clear opportunity to establish large mammalian models of human disease (Eaton and Wishart 2017). However, although significant progress has been made in understanding the morphology of lower mammalian NMJs in several species using modern imaging

techniques, data from larger mammals remains sparse (Tello 1922; Anzenbacher and Zenker 1963; Haddix et al. 2018).

In the present study we sought to establish baseline reference datasets of NMJ morphology across multiple mammalian species (mouse, cat, dog, sheep, pig, human). By utilising our recently-developed NMJ-morph platform for comparative analysis of NMJ morphology (Jones et al., 2016), we have been able to generate comprehensive morphometric NMJ data from lower limb/hindlimb musculature of each species.

Methods

Animals

All animal studies were performed in accordance with the Animals (Scientific Procedures) Act 1986. No animals were sacrificed specifically for this project: tissue was sampled from animals in existing studies (after experimental endpoints had been reached) or from animals submitted for euthanasia (to Dryden Farm or The Roslin Institute). Four mammalian species were investigated: cat (*N* = 3; mean age = 12.6 years), dog (*N* = 3; mean age = 6.6 years), sheep (*N* = 3; mean age = 16 months) and pig (*N* = 3; mean age = 18 months). Full details are provided in **Supplementary Table 1.** In addition, comparative data from mouse (*N* = 3; mean age = 12 weeks) and human (*N* = 21; mean age = 67 years) was obtained from our reference archive (including previously published data; Jones et al. 2017). All previous human studies were covered by the requisite ethics approvals (NHS Lothian REC: 2002/1/22, 2002/R/OST/02; NHS Lothian BioResource: SR719, 15/ES/0094).

Tissue sampling

Animals were euthanised and samples were harvested within 1 hour post-mortem. Three individual animals from each species (cat, dog, sheep, and pig) were sampled. To facilitate cross-species comparison, previously studied muscles were selected (Jones et al. 2017): *extensor digitorum longus, peroneus longus*, *peroneus brevis* and *soleus*. Given the substantial difference in gross anatomy between the species (e.g. dogs lack a *soleus*; sheep and pigs have combined *peronei*) every effort was made to sample equivalent muscles based on standard descriptions of veterinary anatomy (Aspinall and Cappello 2015; Done et al. 2009; König, Horst Erich et al. 2014; Fails and Magee 2018).

Full-length muscle fibres from origin to insertion (2-3 cm in length) were dissected from each of the hindlimb muscles and immediately fixed in 4% paraformaldehyde (PFA) for 3-4 hours. Muscle samples were then washed with 1x phosphate-buffered saline (PBS) and micro dissected into small bundles of 10-15 individual fibres. All remaining fat and connective tissue was removed to reduce potential background staining.

NMJ immunohistochemistry

NMJs were immunolabelled by modifying an established protocol (Jones et al. 2017) to visualize pre-synaptic nerve terminal proteins (SV2 and 2H3) and post-synaptic acetylcholine receptors (AChRs).

Muscle fibres were placed in the following sequence of solutions (made up in 1xPBS unless otherwise specified): glycine (0.1M pH 10.4) for 15 min to reduce tissue auto-fluorescence; 1xPBS wash for 15 min; tetramethylrhodamine α-bungarotoxin (TRITC α-BTX, BTIU00012, VWR International Ltd.) 2 µg/mL for 15 min to label AChRs; 4% Triton X-100 for 1.5 hrs for tissue permeabilization; then a blocking solution of 4% bovine serum albumin (BSA) and 2% Triton X-100 for 30 min. Tissue was then incubated overnight (at room temperature) with the primary antibodies (in blocking solution): mouse monoclonal anti-SV2 IgG (to label synaptic vesicles) and mouse monoclonal anti-2H3 IgG (to label neurofilament) (both at 1:50 dilution; Developmental Studies Hybridoma Bank, University of Iowa). This was followed by 4 x 20 min PBS washes; overnight incubation (at 4°C) with the secondary antibodies (Alexa 488-donkey anti-mouse IgG; 1:400 dilution; A21202, Life Technologies); then 4 x 20 min PBS washes. Muscle samples were finally mounted on glass slides in Mowiol and kept in dark storage to prevent photobleaching.

Confocal imaging & NMJ-morph analysis

NMJ images were acquired on Nikon A1R FLIM and Zeiss Axiovert LSM510 confocal microscopes using established protocols for large volume imaging (Jones et al. 2016; 2017). Muscle fibres were imaged on an Olympus IX71 microscope and Hamamatsu C4742-95 camera with Openlab Improvision software using the same guidelines (Jones et al, 2016; 2017). For each individual muscle (n = 135) an average of 40-60 NMJs/muscle fibres were imaged, where possible. Muscle fibre diameters were measured subsequently from randomly identified fibres using standard light microscopy (Jones et al. 2016; 2017). It was not possible to record correlated NMJ and muscle fibre measurements from single identified fibres.

Image analysis was performed using the standardized 'NMJ-morph' approach to quantify 21 individual morphological variables in each NMJ (including pre- and post-synaptic variables and associated nerve/muscle measurements; Jones et al, 2016; 2017 and Boehm et al, 2020). In total, 5,385 NMJs were analysed across the 6 species, sampled from 135 muscles of 36 individual animals/patients (with mouse and human data pooled from Jones et al. 2017).

Data Availability Statement

All experimental data are contained within the figures and tables. All raw data files (including confocal micrographs and data spreadsheets) are freely available upon request.

Statistical analysis

All statistical analyses were performed in GraphPad Prism Software (Version 8). Individual statistical tests are detailed in main text and figure legends. Statistical significance was considered to be $P < 0.05$.

Results

Building on our recent work reporting marked differences between NMJ morphology in humans and mice (Jones et al. 2017), we initially set out to extend our knowledge of NMJ morphology across a wider range of mammalian species: cat, dog, sheep and pig. Basic background data relating to individual animals used in this study, including source and breed, is provided in Supplementary Table 1.

The choice of muscles for examination (*extensor digitorum longus, peroneus longus*, *peroneus brevis* and *soleus;* EDL, PL, PB and S respectively) was determined by our previously published human and mouse datasets (Jones et al. 2017) as well as their accessibility for dissection. The gross anatomy of hindlimb muscles in cat, dog, sheep and pig (**Figure 1**) does reveal some species-specific differences (e.g. the dog lacks *soleus,* whilst both sheep and pig lack *peroneus brevis*) that likely represent functional and/or evolutionary adaptations. Nevertheless, every attempt was made to source the equivalent muscles in each species based on existing descriptions of veterinary and comparative anatomy (Aspinall and Cappello 2015; Done et al. 2009; König, Horst Erich et al. 2014; Fails and Magee 2018). NMJs from each muscle/species were immunohistochemically-labelled, imaged and subjected to morphometric analyses using NMJ-morph, according to our established protocols (Jones et al, 2016; 2017 and Boehm et al, 2020). In total, 5,385 NMJs were analysed across the 6 species, sampled from 135 muscles of 36 individual animals/patients (with mouse and human reference data obtained from Jones et al. 2017).

Initial qualitative observations revealed marked inter-species heterogeneity of NMJ morphology (Figure 2). Mouse NMJs displayed a typical 'pretzel' shaped morphology, a well-

established observation in multiple previous studies (Marques et al, 2000). In marked contrast, human NMJs were much smaller and possessed a characteristic 'nummular' morphology (Jones et al, 2017). Of the other mammalian species, cat and dog NMJs were striking in their dissimilarity, with cat NMJs being particularly small and dog NMJs being amongst the largest examined (equivalent in size to mouse NMJs). In comparison, sheep and pig NMJs appeared quite similar to one another in overall morphology, and most closely resembled the human NMJs on initial inspection. In addition, and as expected, there was notable variation of individual NMJ morphology within individual muscles (Jones et al, 2016; 2017).

Quantitative NMJ-morph analysis was then performed on the complete dataset of 5,385 NMJs (Figures 3 and 4; Table 1). Pooling NMJ data across all muscles sampled (EDL, PL, PB, S) facilitated a comparison of 'average' NMJ morphology in each species for all 21 individual pre- and post-synaptic variables generated by NMJ-morph (Table 1). Statistical comparison of these values was then performed with reference to our existing human (Jones et al., 2017) dataset.

The majority of core NMJ variables were significantly larger in both mouse (6/11 variables) and dog (10/11 variables) compared to humans; these differences were also matched by significantly greater axonal diameters in both species. At the opposite end of the spectrum, cat NMJs were significantly smaller than human NMJs (in 5/11 core variables). In contrast, quantitative analysis of both sheep and pig NMJs revealed a closer similarity to human NMJs, with the vast majority of variables in both species (19/21 in sheep; 18/21 in pig) showing no statistically significant differences.

To determine whether these observations were reflective of NMJ morphology at the level of individual muscles, datasets from each species were segregated into distinct muscle groups: EDL, PL, PB and S (Figure 4). ~~Compared with the marked variation in 'average' NMJ morphology observed between species (Figures 2 and 3; Table 1) NMJ morphology within identified anatomical muscles from a single species was found to be relatively uniform.~~ Compared with the marked variation in average NMJ morphology between species (Figures 2 and 3; Table 1) the differences that exist between individual muscles within a species (Jones et al. 2016) are much less pronounced. Moreover, there was no overt pattern to suggest a relationship between NMJ morphology and muscle fibre type (e.g. fast-twitch/slow-twitch) or anatomical 'identity' at the whole muscle level. For example, in both humans and mice, the *largest* relative NMJs were found in soleus (an archetypal slow twitch muscle) whereas in sheep and pigs, soleus contained the *smallest* relative NMJs (Figure 4).

We next investigated the relationship between NMJ size and muscle fibre diameter. Previous studies have suggested a significant positive correlation between NMJ size and muscle fibre diameter (Kuno et al. 1971; Harris and Ribchester 1979; Slack et al. 1983; Balice-Gordon and Lichtman 1990), as well as an inverse relationship between NMJ size and body mass (Paul 2001; Slater 2017). We performed a correlation analysis of muscle fibre diameter against each of 18 pre- and post-synaptic NMJ variables across all species (Figure 5). Despite modest correlations for individual variables in some species (e.g. pig and human; Figure 5) no overall relationship was observed for the majority of NMJ variables across the pooled data for all

species. This finding suggests that muscle fibre diameter is not the sole/major determinant of NMJ size and morphology.

Finally, we wanted to determine whether relative body size/mass was contributing to NMJ size/morphology. When taken together with our previous observations, we found no clear relationship between NMJ size/morphology, muscle fibre diameter, and/or body size (Figure 6). For example, the greatest disparity between NMJ size and muscle fibre diameter was observed between the two smallest animals included in the study, with the mouse possessing the largest NMJs on the smallest muscle fibres, and the cat displaying the smallest NMJs on the largest muscle fibres. In contrast, the three largest species by weight (sheep, pig and human) had the most closely matched 'NMJ size/fibre size' pairings, with sheep and humans showing the most similarities.

Discussion

The current study presents comparative reference/baseline data for NMJ morphology across 6 mammalian species (Table 1; Figure 6). We reveal marked species-specific differences in NMJ morphology across a range of anatomically-defined muscle groups in the mammalian lower limb/hindlimb. We report marked heterogeneity of NMJ morphology both within and between species, with no relationship found between NMJ morphology and muscle fibre diameter or body size. Of all the species examined in this study, the sheep NMJ was found to most closely resemble the human NMJ.

The finding of marked heterogeneity in NMJ morphology across a range of mammalian species questions the extent to which NMJ form and function in one species can automatically be translated to our understanding of NMJ form and function in another mammalian species. Whilst there are undoubtedly many aspects of NMJ form and function that have been successfully replicated across mammalian species, it is possible to envisage a scenario whereby responses to degenerative or disease stimuli could elicit distinct species-specific responses at the NMJ. Indeed, this may (at least in part) help to explain why many studies of NMJ-related diseases in mouse models have not been successfully translated to human patients (e.g. in motor neuron diseases such as amyotrophic lateral sclerosis; Dupuis and Loeffler 2009; Clerc et al. 2016). However, this may reflect only one aspect of multi-factorial issues contributing to the poor therapeutic translation of clinical trials (Tosolini and Sleigh 2017; Mitsumoto et al. 2014).

Our finding that pig, and particularly sheep, NMJs more closely resemble human NMJs than those in mice, cats and dogs, suggests that the utilisation of large animal models may be more

appropriate and accurate for understanding human NMJs in health and disease. Indeed, many new spontaneous and genetically-altered large animal models of neurological and neuromuscular disease have recently been reported (Eaton and Wishart 2017). For example, porcine models of spinal muscular atrophy (Walters and Prather 1969; Lorson et al. 2011; Prather et al. 2013; Duque et al. 2015) and ovine models of Batten disease (Weber and Pearce 2013; Eaton et al. 2019) are now both available for basic, pre-clinical and clinical studies. Thus, the incorporation of large mammalian models into research programmes is likely to yield important new insights into NMJ biology, as well as the development of effective therapies for neuromuscular conditions.

Correlation analyses of NMJ morphology and muscle fibre diameter in the present study add significant experimental support to refute the hypothesis that the former is largely dictated by the latter (Kuno et al. 1971; Harris and Ribchester 1979; Slack et al. 1983; Balice-Gordon and Lichtman 1990). Our data therefore support previous studies suggesting a disconnection of NMJ morphology and muscle fibre size in rodents, primates and humans (Anzenbacher and Zenker 1963; Jones et al. 2017). However, it is important to note that this observation is distinct from the relationship that has been shown to exist between the size of an NMJ and its corresponding muscle fibre when undergoing atrophy and hypertrophy in situations of muscle wasting, exercise or hormonal manipulation (e.g. as has been reported in the mouse bulbocavernosus muscle; Balice-Gordon and Lichtman 1990). It remains unclear, therefore, as to which factors directly determine NMJ morphology in vivo, although recent studies have suggested that the identity of the motor neuron itself is likely to exert a strong influence (Jones et al. 2016; 2017).

Given that muscle fibre diameter does not determine the *absolute* size/morphology of any given NMJ it appears that the 'ratio' between NMJ size and muscle fibre diameter represents a unique characteristic in each species, and one that is furthermore independent of body mass (Figure 6). This notion was previously proposed for different muscles within the rat (Oda 1985), but here we extend these findings to show that it persists across multiple mammalian species.

Acknowledgements

The mouse SV2 and 2H3 monoclonal antibodies, developed by Buckley, K.M. and Jessell, T.M. / Dodd, J. respectively, were obtained from the Developmental Studies Hybridoma Bank, created by the NICHD of the NIH and maintained at The University of Iowa, Department of Biology, Iowa City, IA 52242. This study was supported by a Prize PhD Studentship from the Anatomical Society (to IB & THG), small project grant funding from Anatomy@Edinburgh (to RAJ & THG) and a travelling scholarship (to ASL) from Coordenação de Aperfeiçoamento de Pessoal de Nível Superior – Brasil (CAPES).

Author contributions

IB, RAJ and THG conceived and designed the study. IB, AA, ASL, AG, OM, RF, RAJ and THG performed experiments and analysed data. CL, RP, CP, RC and TMW provided access to, and guidance with, tissue sampling. AB, AA, ASL, RAJ and THG wrote the manuscript. All authors edited and approved the manuscript.

References

Anzenbacher H, Zenker W. Über die Grössenbeziehung der Muskelfasern zu ihren motorischen Endplatten und Nerven. *Zeitschrift für Zellforschung und Mikroskopische Anatomie*.: 1963; 60(6):860-871

Aspinall, V., & Cappello, M. Introduction to Veterinary Anatomy and Physiology Textbook (M. Cappello (ed.); Third edition) [Book].: 2015 *Elsevier*.

Balice-Gordon RJ, Lichtman JW. In vivo visualization of the growth of pre- and postsynaptic elements of neuromuscular junctions in the mouse. *Journal of Neuroscience*.: 1990; 10(3):984-908.

Boehm, I., Miller, J., Wishart, T. M., Wigmore, S. J., Skipworth, R. J. E., Jones, R. A., & Gillingwater, T. H. Neuromuscular junctions are stable in patients with cancer cachexia. *JCI*.: 2020; 130(3), 1461–1465.

Clarac F, Pearlstein E. Invertebrate preparations and their contribution to neurobiology in the second half of the 20th century. *Brain Res Rev*.: 2007; 54(1):113–61.

Clerc P, Lipnick S, Willett C. A look into the future of ALS research. *Drug Discov Today*.: 2016; 21(6):939–49.

Done SH, Goody P, Stickland S, Evans N. Color atlas of veterinary anatomy. Volume 3: the dog and cat. 2009; *Mosby/Elsevier*;

Dupuis L, Loeffler J-P. Neuromuscular junction destruction during amyotrophic lateral sclerosis: insights from transgenic models. *Curr Opin Pharmacol*.: 2009; 9(3):341–6.

Duque SI, Arnold WD, Odermatt P, Li X, Porensky PN, Schmelzer L, et al. A large animal model of spinal muscular atrophy and correction of phenotype. *Ann Neurol*.: 2015;

77(3):399–414.

Eaton SL, Proudfoot C, Lillico SG, Skehel P, Kline RA, Hamer K, et al. CRISPR/Cas9 mediated generation of an ovine model for infantile neuronal ceroid lipofuscinosis (CLN1 disease). *Sci Rep*.: 2019; 9(1).

Eaton SL, Wishart TM. Bridging the gap: large animal models in neurodegenerative research. *Mamm Genome*.: 2017; 28(7–8):324–37.

Fails AD, Magee C. Anatomy and Physiology of Farm Animals. *The Canadian Veterinary Journal*.: 2018; 7(11):267. Hoboken, NJ, USA: Wiley Blackwell;

Haddix SG, Lee Y Il, Kornegay JN, Thompson WJ. Cycles of myofiber degeneration and regeneration lead to remodeling of the neuromuscular junction in two mammalian models of Duchenne muscular dystrophy. *PLoS One*.: 2018; 13(10):1–24.

Harris JB, Ribchester RR. The relationship between end-plate size and transmitter release in normal and dystrophic muscles of the mouse. *J Physiol*.: 1979; 296(1):245–65.

Jones RA, Harrison C, Eaton SL, Llavero Hurtado M, Graham LC, Alkhammash L, et al. Cellular and Molecular Anatomy of the Human Neuromuscular Junction. *Cell Rep*.: 2017; 21(9):2348–56.

Jones RA, Reich CD, Dissanayake KN, Kristmundsdottir F, Findlater GS, Ribchester RR, et al. NMJ-morph reveals principal components of synaptic morphology influencing structure–function relationships at the neuromuscular junction. *Open Biol*.: 2016; 6(12):160240.

König, Horst Erich, Liebich H-G, Aurich C, Weller R. *Veterinary anatomy of domestic mammals: textbook and colour atlas. Sixth edition*.: 2014; Stuttgart: Schattauer;

Kuno M, Turkanis SA, Weakly JN. Correlation between nerve terminal size and transmitter release at the neuromuscular junction of the frog. *The Journal of Physiology*.: 1971;

213(3):545-555

Lorson MA, Spate LD, Samuel MS, Murphy CN, Lorson CL, Prather RS, et al. Disruption of the Survival Motor Neuron (SMN) gene in pigs using ssDNA. *Transgenic Res*.: 2011; 20(6):1293–304.

Marques MJ, Conchello JA, Lichtman JW. From Plaque to Pretzel: Fold Formation and Acetylcholine Receptor Loss at Developing Neuromuscular Junctions. *The Journal of Neuroscience*: 2000; 20:3663-3675.

Mitsumoto H, Brooks BR, Silani V. Clinical trials in amyotrophic lateral sclerosis: Why so many negative trials and how can trials be improved? *Lancet Neurol*.: 2014; 13(11):1127–38.

Murray LM, Talbot K, Gillingwater TH. Review: Neuromuscular synaptic vulnerability in motor neurone disease: Amyotrophic lateral sclerosis and spinal muscular atrophy. *Neuropathol Appl Neurobiol*.: 2010; 36(2):133–56.

Oda K. The Relationship between Motor Endplate Size and Muscle Fibre Diameter in Different Muscle Groups of the Rat. *Japanese Journal of Physiology*: 1985; 35:1091-1095.

Paul AC. Muscle length affects the architecture and pattern of innervation differently in leg muscles of mouse, guinea pig, and rabbit compared to those of human and monkey muscles. *Anat Rec*.: 2001; 262(3):301–9.

Prather RS, Lorson M, Ross JW, Whyte JJ, Walters E. Genetically Engineered Pig Models for Human Diseases. *Annu Rev Anim Biosci*.: 2013; 1(1):203–19.

Rodríguez Cruz P, Palace J, Beeson D. The Neuromuscular Junction and Wide Heterogeneity of Congenital Myasthenic Syndromes. *Int J Mol Sci*.: 2018; 19(6):1677.

Rudolf R, Deschenes MR, Sandri M. Neuromuscular junction degeneration in muscle

wasting. *Curr Opin Clin Nutr Metab Care*.: 2016; 19(3):177–81.

Rudolf R, Khan MM, Witzemann V. Motor Endplate—Anatomical, Functional, and Molecular Concepts in the Historical Perspective. *Cells*.: 2019; 8(5):387.

Slack JR, Pockett S, MacClement BAE. Regulation of postnatal growth of motor end plates in rat soleus muscle. *Exp Neurol*.: 1983; 80(2):321–8.

Slater CR. Structural factors influencing the efficacy of neuromuscular transmission. *Ann N Y Acad Sci*.: 2008; 1132:1–12.

Slater CR. The functional organization of motor nerve terminals. *Prog Neurobiol*.: 2015; 134:55–103.

Slater CR. The structure of human neuromuscular junctions: Some unanswered molecular questions. *Int J Mol Sci*.: 2017; 18(10):2183.

Szule JA, Jung JH, McMahan UJ. The structure and function of "active zone material" at synapses. *Philos Trans R Soc Lond B Biol Sci*.: 2015; 370(1672):20140189.

Tello JF. Die Entstehung der motorischen und sensiblen Nervenendigungen: I. In dem lokomotorischen Systeme der höheren Wirbeltiere. Muskuläre Histogenese. *Z Anat Entwicklungsgesch*.: 1922; 64(4–6):348–440.

Verschuuren J, Strijbos E, Vincent A. Neuromuscular junction disorders. *Handbook of Clinical Neurology*.: 2016; 447–66.

Walters EM, Prather RS. Advancing swine models for human health and diseases. *Mo Med*.: 1969; 110(3):212–5.

Weber K, Pearce DA. Large animal models for batten disease: A review. *J Child Neurol*.: 2013; 28(9):1123–7.

Wood SJ, Slater CR. Safety factor at the neuromuscular junction. *Progress in Neurobiology*.: 2001; 64:393-429.

1

2

Figure Legends

Figure 1. Gross anatomy of hindlimb muscles in cat, dog, sheep, and pig

Representative photographs illustrating gross muscle morphology in each species. The proximal end of the limb is on the right-hand side of the image. A block of tissue containing full-length muscle fibres (from origin to insertion) was sampled from each of the selected muscles. Note the species-specific absence of certain muscles – dog lacks *soleus,* sheep and pig lack *peroneus brevis***.** EDL: *Extensor Digitorum Longus*; PL: *Peroneus Longus*; PB: *Peroneus Brevis*; SOL: *Soleus.* Scale bar = 2 cm.

Figure 2. Heterogeneity of mammalian NMJs

Representative confocal micrographs of 'average' NMJs from each species (ranked according to body mass). The selected NMJ images most closely represent the 'average' morphology (size, shape) across the limb muscles sampled (EDL, soleus, peronei). Mouse NMJs are typically 'pretzel' shaped; human NMJs have a 'nummular' morphology. Of the species represented, sheep and pig NMJs appear most similar to human NMJs. Images have been pseudo-coloured for display purposes; all analysis has been performed on grayscale images. SV2/2H3 = synaptic vesicle and neurofilament (green); α-BTX (α-bungarotoxin) = acetylcholine receptors (magenta). Scale bar = 20 µm (across all images).

Figure 3. NMJ-morph analysis reveals inter-species variations in NMJ morphology

Comparison of 'average' NMJ morphology in each species for a range of pre- and post-synaptic variables. Data for each morphological variable is pooled by muscle identity (EDL, PL, PB, S) for each species and statistical comparison is made with the human NMJ. Boxes contain the mean (+) and median (line) values for each NMJ variable and extend from the 25th to 75th percentiles, with the whiskers representing the maximum and minimum values. Compared to humans, mouse and dog NMJs are significantly larger, with equivalent differences in axon calibre. In contrast, sheep and pig NMJs are the most similar to humans, with the majority of NMJ variables showing no significant differences between the species (see also **Supplementary Table 1)**. In total, 5,385 individual NMJs were analysed [Cat: N = 3 animals, n = 12 muscles, 465 NMJs; Dog: N = 3, n = 9, 341 NMJs; Sheep: N = 3, n = 9, 313 NMJs; Pig: N = 3, n = 9, 446 NMJs; Mouse: N = 3, n = 24, 960 NMJs; Human: N = 21, n = 72, 2860 NMJs. Mouse

and human data from Jones et al. 2017]**.** *One–way ANOVA with Dunnett's post hoc analysis (for parametric variables) and Kruskal-Wallis test with Dunn's post hoc analysis (for non-parametric variables)* *p < 0.05; **p < 0.01; ***p < 0.001; ****p < 0.0001.

Figure 4. NMJ-morph analysis of inter-muscle variations in NMJ morphology

The pooled data in Figure 3 has been segregated to demonstrate 'average' NMJ morphology for individual muscles (EDL, PL, PB, S). Compared with the marked inter-species variation, the differences between individual muscles are much less pronounced.

Figure 5. No significant relationship between NMJ morphology and muscle fibre diameter

Scatterplots demonstrating the correlation between size-related NMJ variables and muscle fibre diameter. Each data point represents an individual muscle (mean of 40 NMJs / 40 muscle fibres). Despite modest correlations for some variables, there is no significant relationship between NMJ size and muscle fibre diameter across the species investigated. Mouse = purple circles; Cat = green squares; Dog = blue triangles; Sheep = orange diamonds; Pig = black stars; Human = grey circles. *Correlation coefficients (Pearson) are for individual species (within the box) and all species pooled (above the box).* $^{*}p < 0.05$; $^{**}p < 0.01$; $^{***}p < 0.001$.

Figure 6. Schematic overview of NMJ morphology, muscle fibre diameter, and body size

Schematic diagram illustrating the relationship between NMJ size, muscle fibre diameter and body weight. For each species, the mean values for AChR area and muscle fibre diameter are depicted (Table 1) to provide an accurate visual representation of inter-species differences/similarities. Of the species investigated, the starkest contrast is between the two smallest animals; the mouse has the largest NMJs on the smallest muscle fibres, the cat has the smallest NMJs on the largest muscle fibres. Sheep and pig are most similar to human, with sheep and human bearing the closest resemblance. Overall, there is no relationship between NMJ size, muscle fibre diameter and body mass; the ratio between NMJ size and muscle fibre diameter is therefore unique to each species. Scale bar = 20 µm.

1

1 **Table 1**

	Mouse N = 3, n = 24 960 NMJs	Cat N = 3, n = 12 465 NMJs	Dog N = 3, n = 9 341 NMJs	Sheep N = 3, n = 9 313 NMJs	Pig N = 3, n = 9 446 NMJs	Human N = 21, n = 72 2860 NMJs
Core variables						
pre-synaptic						
1) *Nerve Terminal Area (µm²)*	304.0**** ± 11.7	98.5 ± 5.4	305.1*** ± 24.9	153.9 ± 14.3	197.6 ± 24.7	122.7 ± 5.98
2) *Nerve Terminal Perimeter (µm)*	327.4**** ± 9.4	272.1*** ± 13.9	441.0**** ± 31.7	231.7* ± 12.3	234.7* ± 18.6	151.1 ± 6.53
3) *Number of Terminal Branches*	30.0 ± 1.2	101.4**** ± 7.4	95.6**** ± 8.5	45.5 ± 4.4	40.0 ± 6.0	28.0 ± 1.40
4) *Number of Branch Points*	26.0 ± 0.9	57.6*** ± 6.9	62.9**** ± 3.5	26.4 ± 2.6	38.5* ± 3.2	14.0 ± 0.85
5) *Total Length of Branches (µm)*	166.7**** ± 4.8	128.7** ± 7.7	215.7**** ± 13.5	109.5 ± 8.1	134.5** ± 12.0	69.3 ± 3.28
post-synaptic						
6) *AChR Area (µm²)*	424.2*** ± 14.1	159.6 ± 9.3	420.8*** ± 35.1	182.2 ± 14.0	239.5 ± 25.2	206.7 ± 8.0
7) *AChR Perimeter (µm)*	275.8** ± 8.8	332.7**** ± 16.5	536.5**** ± 41.7	241.6* ± 15.2	221.7 ± 18.6	152.2 ± 5.8
8) *Endplate Area (µm²)*	678.2*** ± 24.3	333.2 ± 19.9	858.9**** ± 85.0	365.4 ± 16.8	384.2 ± 38.5	351.5 ± 14.4
9) *Endplate Perimeter (µm)*	118.8 ± 2.9	91.4 ± 3.0	139.1** ± 10.2	85.1 ± 3.8	95.5 ± 7.3	98.7 ± 2.6
10) *Endplate Diameter (µm)*	42.2 ± 1.2	30.9 ± 1.1	48.1** ± 3.4	30.3 ± 1.4	32.2 ± 2.0	36.0 ± 0.9
11) *Number of AChR Clusters*	2.6 ± 0.2	3.2 ± 0.4	3.8 ± 0.5	4.9 ± 0.4	3.7 ± 0.5	3.9 ± 0.2
Derived variables						
pre-synaptic						
12) *Average Length of Branches (µm)*	6.7**** ± 0.2	1.4 ± 0.1	2.6 ± 0.2	3.0 ± 0.4	4.4 ± 0.6	3.0 ± 0.1
13) *Complexity*	4.9 ± 0.1	5.7** ± 0.1	5.9** ± 0.1	4.9 ± 0.1	5.1 ± 0.1	4.1 ± 0.1
post-synaptic						
14) *Average Area of AChR Clusters (µm²)*	238.5**** ± 8.5	75.8 ± 8.6	175.4**** ± 12.6	54.8 ± 6.8	113 ± 12.9	71.7 ± 2.7
15) *Fragmentation*	0.40 ± 0.0	0.51 ± 0.0	0.53 ± 0.1	0.67 ± 0.0	0.48 ± 0.0	0.58 ± 0.0
16) *Compactness (%)*	64.4 ± 0.6	49.5 ± 1.1	50.4 ± 1.8	51.0 ± 3.1	64.5 ± 2.3	61.6 ± 0.6

17) *Overlap (%)*	64.2	±	0.5	45.9	±	1.1	53.1	±	1.1	66.4	±	3.0	71.1	±	3.6	49.6	±	1.1
18) *Area of Synaptic Contact (µm²)*	267.9****	±	9.5	72.4	±	4.5	224.4**	±	18.1	122.0	±	13.4	175.0	±	24.2	105.2	±	5.1
Associated nerve & muscle variables																		
19) *Axon Diameter (µm)*	3.1****	±	0.1	0.96	±	0.1	1.8****	±	0.22	1.1	±	0.09	1.2	±	0.1	0.84	±	0.0
20) *Muscle Fibre Diameter (µm)*	40.2*	±	0.5	84.3**	±	3.5	77.2	±	3.33	63.0	±	3.29	76.6	±	6.7	59.9	±	2.1
21) *Number of Axonal Inputs*	1.0	±	0.0	1.0	±	0.0	1.0	±	0.00	1.0	±	0.00	1.1	±	0.1	1.0	±	0.0

Table 1. Baseline morphological data for the mammalian NMJ – 6 species

Complete NMJ-morph data for the 6 species. Values are the mean (± SEM) for each NMJ variable pooled across all muscles sampled (EDL, PL, PB, S) in each species. N = individual animals; n = individual muscles; total NMJs per species listed below. All statistical comparisons performed in relation to the human data; one–way ANOVA with Dunnett's post hoc analysis (parametric variables) and Kruskal-Wallis test with Dunn's post hoc analysis (non-parametric variables). *p < 0.05; **p < 0.01; ***p < 0.001; ****p < 0.0001. No asterisk indicates non-significant result. Mouse and human data reproduced from Jones et al, 2017.

1

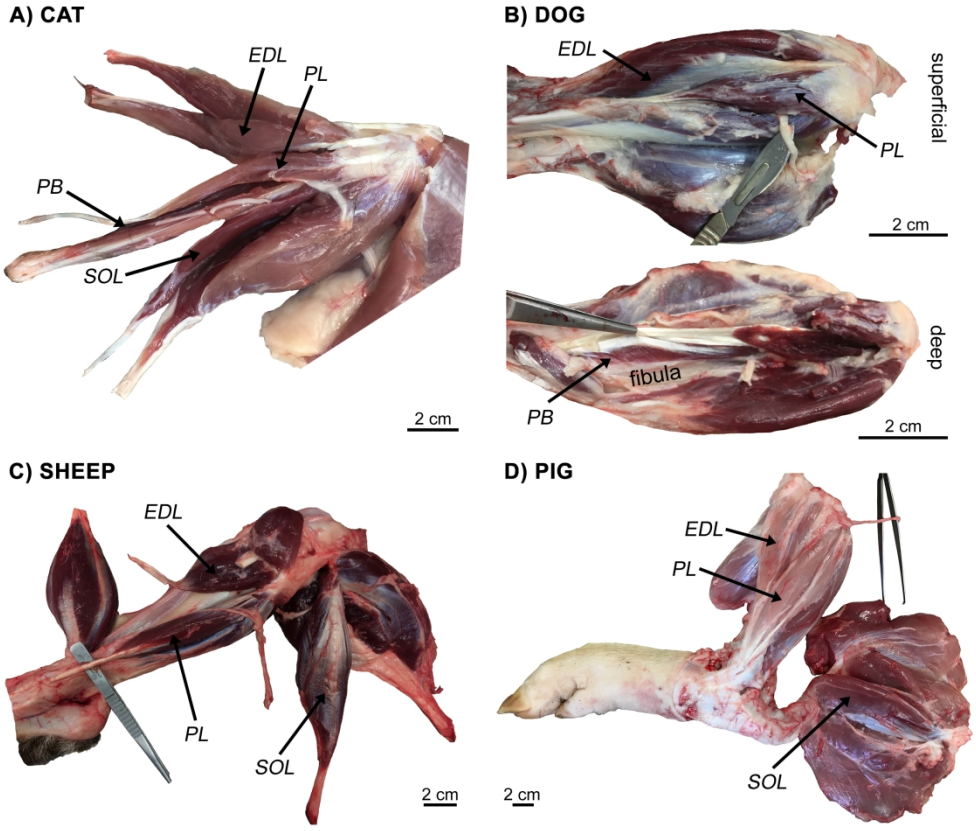

Figure 1

227x190mm (300 x 300 DPI)

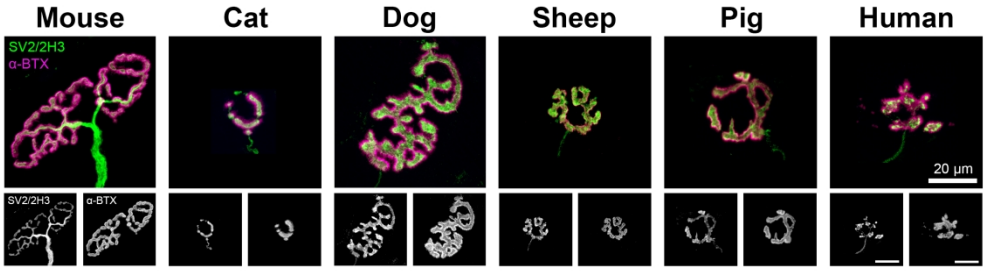

Figure 2

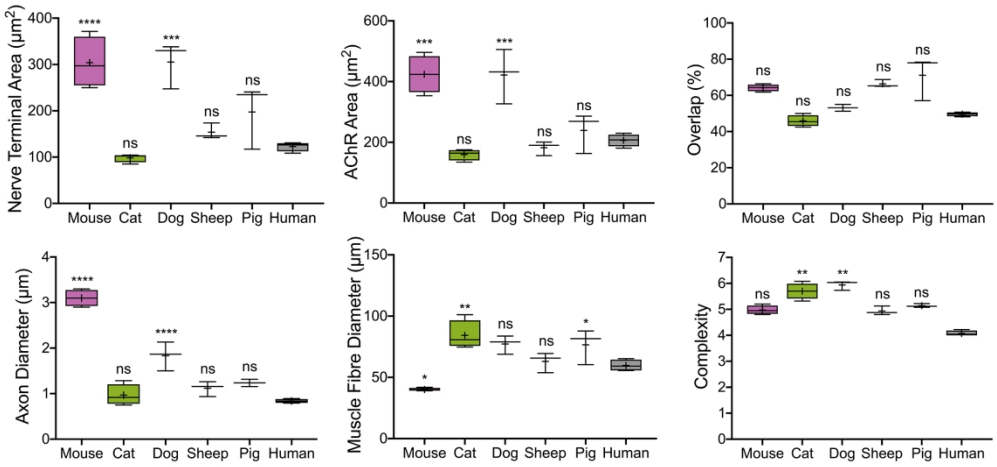
Nerve Terminal Area (µm²)
AChR Area (µm²)
Overlap (%)
Axon Diameter (µm)
Muscle Fibre Diameter (µm)
Complexity
Mouse Cat Dog Sheep Pig Human
****
***
**
*
ns

Figure 3

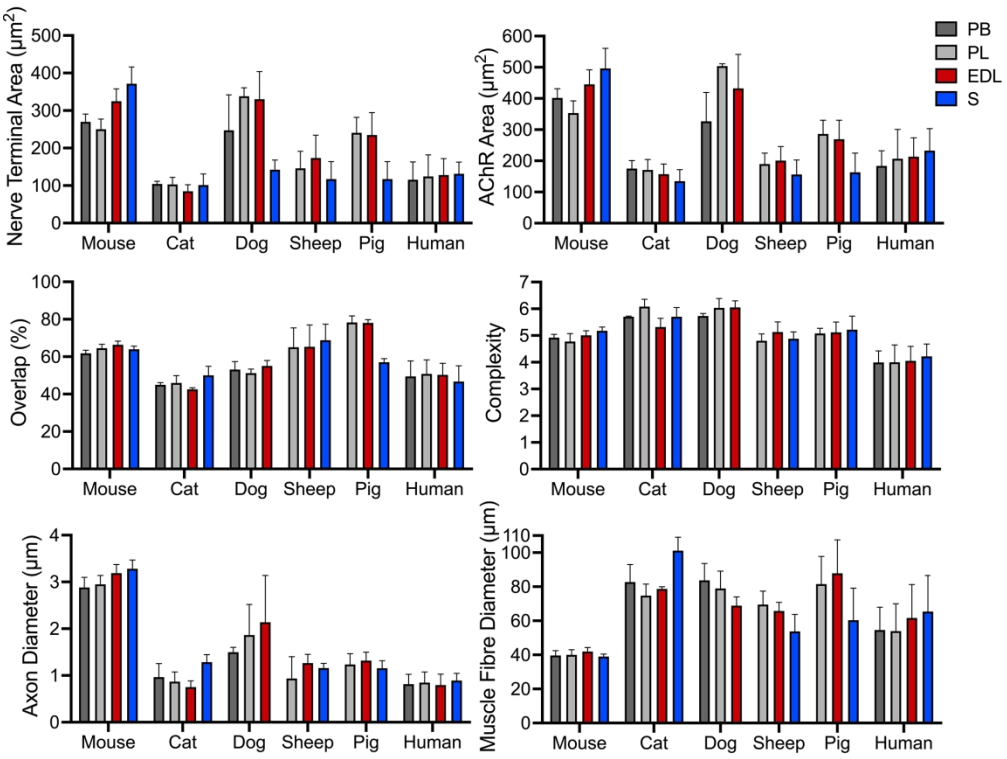

Figure 4

100x76mm (600 x 600 DPI)

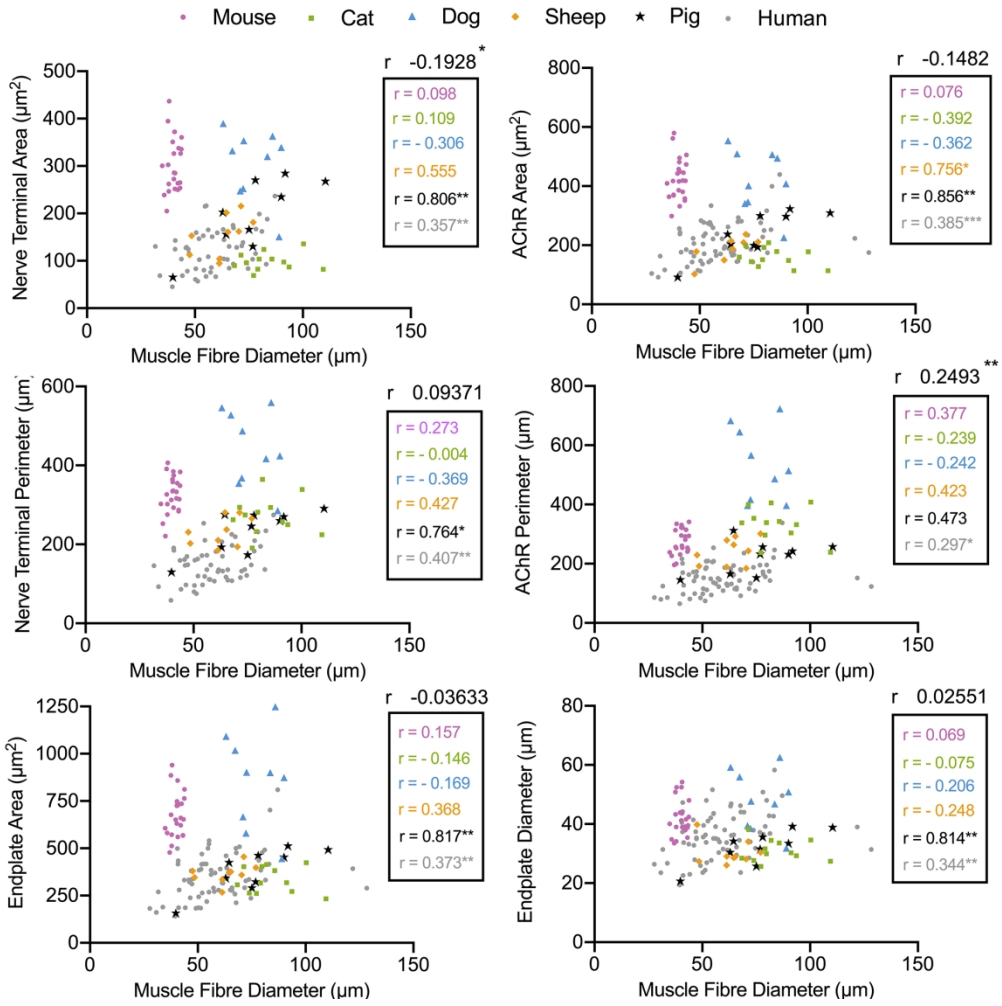
Mouse
Cat
Dog
Sheep
Pig
Human
Nerve Terminal Area (µm²)
r -0.1928*
r = 0.098
r = 0.109
r = - 0.306
r = 0.555
r = 0.806**
r = 0.357**
AChR Area (µm²)
r -0.1482
r = 0.076
r = - 0.392
r = - 0.362
r = 0.756*
r = 0.856**
r = 0.385***
Nerve Terminal Perimeter (µm)
r 0.09371
r = 0.273
r = - 0.004
r = - 0.369
r = 0.427
r = 0.764*
r = 0.407**
AChR Perimeter (µm)
r 0.2493**
r = 0.377
r = - 0.239
r = - 0.242
r = 0.423
r = 0.473
r = 0.297*
Endplate Area (µm²)
r -0.03633
r = 0.157
r = - 0.146
r = - 0.169
r = 0.368
r = 0.817**
r = 0.373**
Endplate Diameter (µm)
r 0.02551
r = 0.069
r = - 0.075
r = - 0.206
r = - 0.248
r = 0.814**
r = 0.344**
Muscle Fibre Diameter (µm)

Figure 5

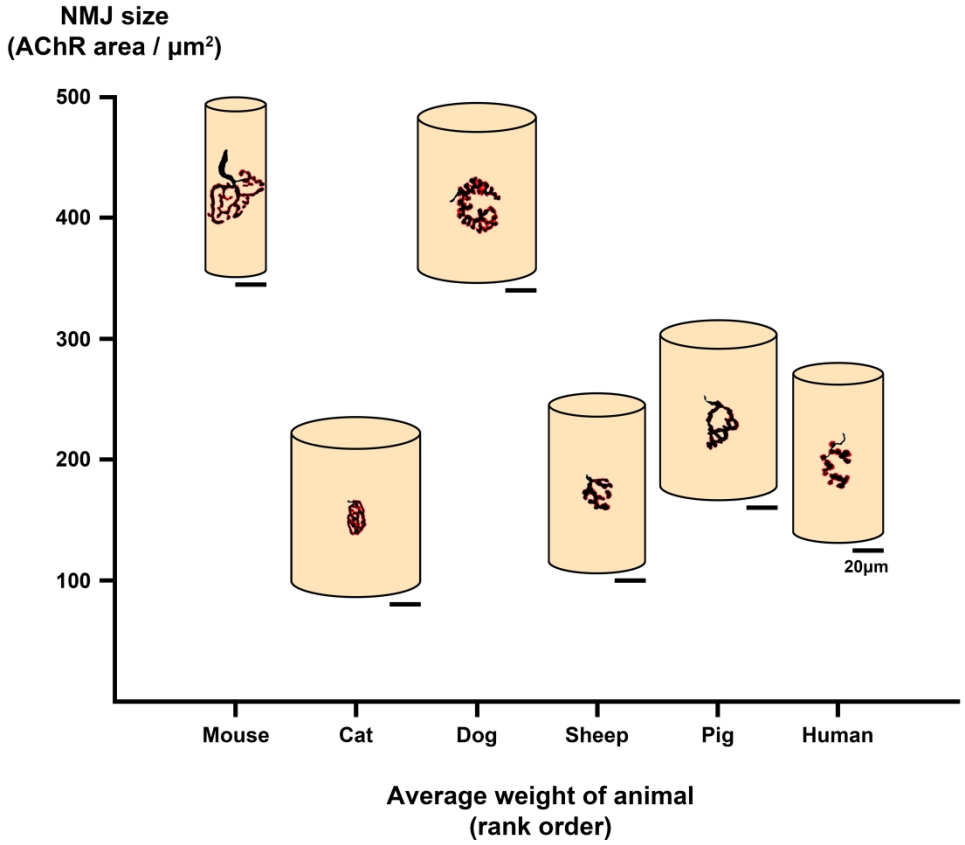
NMJ size
(AChR area / μm²)
500
400
300
200
100
20μm
Mouse
Cat
Dog
Sheep
Pig
Human
Average weight of animal
(rank order)

Figure 6

Boehm et al., Supplementary Table 1

Species	Mouse	Cat	Dog	Sheep	Pig
Sex (M:F)	0:3	0:3	2:1	3:0	0:3
Age	12 weeks	12.6 ± 3.1 years (min 12, max 16)	6.6 ± 4.6 years (min 4, max 12)	1.3 ± 0.2 years (min 1.3, max 1.5)	0.34 years (min 0.33, max 0.35)
Weight	≃ 19 g	4.3 ± 1.4 kg (min 3.2, max 5.3)	≃ 39 kg	75 kg	75.6 ± 7.5 kg (min 67, max 80)
Breed	CD1	Domestic short-haired	Labrador, Staffie X, Lurcher	Texel crosses	Largewhite X landrace
Sampled muscles	EDL, PL, PB, S	EDL, PL, PB, S	EDL, PL, PB	EDL, PL, S	EDL, PL, S
Reason for cull	Experimental	Aggression, hyperthyroidism, chronic kidney disease	Aggression, neoplasia, joint pain	Colony management	Colony management

Supplementary Table 1. Background data of study animals

All species sourced from the animal facilities at the University of Edinburgh (Centre for Discovery Brain Sciences; Roslin Institute; Dryden Farm). Ages for each animal/species equivalent to adulthood. Numerical data are mean ± standard deviation (SD). EDL: *Extensor Digitorum Longus*. PL: *Peroneus Longus*. PB: *Peroneus Brevis*. S: *Soleus*